Journal of Electronic Materials, Vol. 20, No. 1, 1991

Confirmation of Large Lattice Relaxation of the *DX* Center by Extended Photo-Ionization Cross-Section Measurements

G. A. NORTHROP and P. M. MOONEY

International Business Machines Corporation Research Division
Thomas J. Watson Research Center, P.O. Box 218, Yorktown Heights, NY 10598

Although the large lattice relaxation model (LLR) for electron capture at the donor related *DX* center in $Al_xGa_{1-x}As$ has seen wide acceptance over the last 12 years, there have been some recent proposals which have attempted to explain the experimental data with models that only require small lattice relaxation (SLR). One key piece of evidence supporting LLR is the large observed difference (in the case of Si-doped $Al_xGa_{1-x}As$) between the optical (~1.4 eV) and thermal (~0.2 eV) ionization energies. The SLR model proposed that the lowest energy optical ionization was a very weak process, and that the optical transition which had been observed previously is a transition to a higher band. These arguments were supported by photoconductivity data showing a finite photo-ionization rate at energies as low as 200 meV. To resolve this question we have measured the photo-ionization cross section over 7 to 8 orders of magnitude using a tunable infrared laser as a source. A consistent optical ionization energy of about 1.4 eV was observed for 4 samples of differing alloy compositions and doping levels. *In no case was there any detectable photo-ionization below 0.8 eV.* A detailed discussion of these experiments examines the difficulty in obtaining such a large dynamic range optical spectrum. Of particular relevance are the issues of ionization detection, and the brightness of purity of the optical source. A thorough review of these issues and their impact on previous studies of the *DX* center is presented.

Key words: AlGaAs, *DX* centers, lattice relaxation model

INTRODUCTION

$GaAs/Al_xGa_{1-x}As$ heterostructures constitute one of the most frequently examined semiconductor epitaxial systems, primarily due to the close lattice matching of GaAs and AlAs. However, potential applications of this system (and other III-V systems) are complicated by the difficulty in doping $Al_xGa_{1-x}As$ with *n*-type dopants, most of which, such as Si, Sn, and Te have proved simple and effective in GaAs. For Al compositions above ~0.2 the free electron concentration of *n*-type $Al_xGa_{1-x}As$ is lower than the doping level, due to electron trapping at a deep level.[1-3] This trap has subsequently been found to scale in concentration with the doping level,[4-6] thus the root of the term *DX* center, based upon the hypothesis that it resulted from complexing of the dopant with another unknown defect.[7] Moreover the *DX* center seemed to be of considerable scientific interest in that it caused persistent photo-conductivity at low temperatures, indicating a barrier to capture as well as emission of electrons.[8] More recent developments in the field include the observation of the *DX* phenomena in GaAs (both as a band-resonant state in heavily doped material[9] and as a state in the gap under hydrostatic pressure[10-12]), theoretical work indicating that the *DX* state is the result of a shallow to deep transition of the isolated *n*-type dopant,[13] and the currently unresolved question of whether or not *DX* is a negative-*U* center.[13-15] Thus there are both technological and scientific motivations to explore the electronic, optical, and structural properties of this defect.

While the term *DX* center was coined 12 years ago in reference to electron trapping in *n*-type $Al_xGa_{1-x}As$,[7] the earliest indication of unusual electron trapping in *n*-type III-V alloy semiconductors came from studies of S-doped $GaAs_{1-x}P_x$ by Craford *et al.*[16] At temperatures below 100 K they observed persistent photoconductivity for sub-gap excitation of vapor-transport-grown *n*-type $GaAs_{1-x}P_x$ samples of alloy content $x > 0.45$. They interpreted this phenomena as resulting from a barrier to re-capture of the optically excited electrons at the substitutional sulfur donors. They also demonstrated that this nonequilibrium free carrier distribution could be induced either by optical excitation after cooling in the dark, or by rapid thermal quenching in the dark. Although they clearly and correctly elucidated the phenomena, lattice relaxation was not proposed as a mechanism for this barrier to capture until almost 10 years later.

This paper will present a brief overview of the history of optical studies of the *DX* center, with a particular emphasis on the role of optical transitions in delineating the involvement of lattice relaxation in the processes of capture and emission of electrons at this defect. The first section is a brief review of the pioneering work of Lang and co-workers,[7,17-20] with a particular emphasis on the issue of the energy required to optically ionize the deep state. This will include their proposal that the concept of a large lattice relaxation around the center upon electron capture/emission could explain the experi-

(Received June 15, 1990; revised September 20, 1990)

0361-5235/1991/1401-13$5.00©91 AIME

mental phenomena. Next, a more recent body of work from Henning and co-workers[21–25] on the optical properties of *DX* will be reviewed. They presented data for Si-doped $Al_xGa_{1-x}As$ which indicated that the optical ionization energy was much lower than previously thought, allowing the possibility of explaining the *DX* center kinetics without invoking large lattice relaxation. Finally we present extensive photoionization measurements from several Si-doped $Al_xGa_{1-x}As$ samples, all of which show *no evidence for photoionization at low energies*.[26] The photoionization cross section σ_n^o for *DX* was observed to decrease monotonically over as much as eight orders of magnitude, becoming unobservable below 0.8 eV. The last section will describe the difficulties in reliably obtaining such a large dynamic range, and will detail a unique tunable infra-red laser system used in the experiments.

THE PHOTOIONIZATION CROSS SECTION σ_n^o AND LANG'S LARGE LATTICE RELAXATION MODEL

An experimental picture of electron trapping at the *DX* center developed by Lang *et al.*[7] is shown in Fig. 1. This picture shows *DX* as a deep trap at an equilibrium energy E_H below the free electron band edge. For the Si *DX* center this depth, determined by measurements of the temperature dependence of the free carrier concentration (Hall resistivity), varies with alloy composition and has a maximum value of about 160 meV at the direct to indirect gap crossover composition.[23] What makes this defect unusual, of course, is that it presents a barrier of height E_b to the capture of a free electron. This barrier results in persistent photo-conductivity, similar to that seen previously in $GaAs_{1-x}P_x$.[16] At low temperatures, electrons which are optically excited from the bound state into the conduction band lack sufficient thermal energy to surmount this barrier and be recaptured. As the temperature is raised, thermally activated capture begins to take place. The temperature dependence of this capture rate provides a straight-forward means of measuring the barrier height.[8,19] For the Si related *DX* center E_b is found to vary with alloy composition with a minimum value of 210 meV at the direct to indirect gap crossover composition.[27] Finally, since there is a barrier to capture, the thermal emission energy E_c is not the same as the equilibrium energy depth, E_H, but should be the sum of E_H and E_b. The emission energy E_e has been measured directly by DLTS to be 430 meV for the Si related center independent of $0.22 \leq x \leq 0.74$.[27] The Sn and Te related *DX* centers behave similarly, although the capture and emission energies are smaller than for Si.[19]

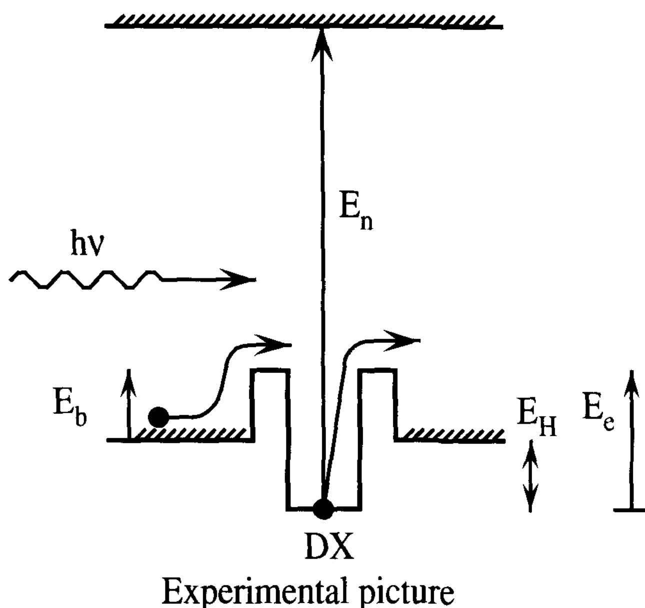

Fig. 1 — Real-space picture of electron trapping at the *DX* center from Lang *et al.*[17] The hatched lines represent a free electron in the conduction band, E_H the equilibrium energy depth of *DX*, and E_b and E_e the thermal capture and emission energies, respectively.

Based upon the thermally derived characteristics of the *DX* center outlined above, large lattice relaxation is only one of several possible mechanisms for a capture barrier. However, the addition of optical transitions to the picture in Fig. 1 provide strong evidence that large lattice relaxation is involved in the ionization process. The two principal observations are: (1) that the optical capture cross section (capture with the emission of a photon) is unobservably small, and (2) that the optical ionization energy is much larger than the thermal binding energy. The reason contrasting optical to thermal measurements has import on the question of lattice relaxation is that purely optical transitions must occur for a fixed lattice configuration, whereas thermal (multi-phonon) processes can account for changes in both energy and lattice configuration.

The lack of any observable optical capture process for the *DX* center is a striking effect. The slow rate of persistent photoconductivity decay at low temperatures puts an upper limit of 10^{-30} cm^{-2} for the optical capture cross section,[18] which should provide the limiting low temperature cross section. This suggests that capture must be a heavily phonon assisted process. The opposite process, that of optical excitation from the bound to free state, or photoionization, is the final key piece of evidence for strong lattice relaxation. The energy of this transition, labeled E_n in Fig. 1, is much larger than the binding or thermal emission energies. This was first determined by a measurement of the photoionization cross section σ_n^o by Lang *et al.*[7,17] for the Te, Sn and Si related *DX* centers. Their data, presented in Fig. 2 as the photoionization cross section vs. photon energy, shows a clear threshold which depends upon the dopant species. Such spectra are typical of what is expected for defect level to band transitions,[28] *except that the energy required is much larger than the corresponding thermal ionization energy*. The curves show thresholds of around 600 and 800 meV and achieve maximum values around 1.1 and 1.3 eV for

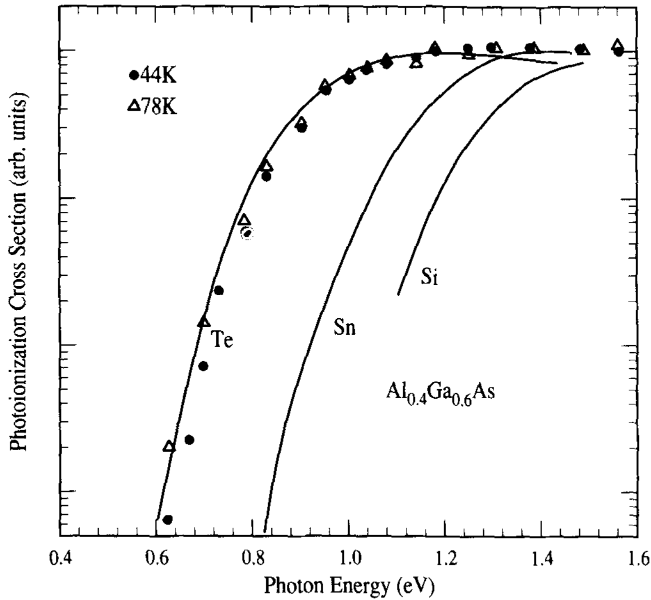

Fig. 2 — Photoionization cross sections from Lang *et al.*[7,17]

Te and Sn, respectively. In the case of Si, the data is not as extensive, but extrapolation puts the threshold at about 900 meV, while the peak cross section is not reached at 1.4 eV, the transmission limit of the GaAs substrate. Thus an optical ionization of ~1.0 eV is in stark contrast to a thermal emission energy of 0.43 eV and a binding energy of ~0.16 eV.

The combination of thermal and optical data led Lang *et al.* to propose that large lattice relaxation could explain the behavior of the *DX* center.[7,17,18] This model is presented in a simple form in Fig. 3, labeled with the transitions discussed above. The horizontal axis in this diagram is a configuration coordinate, which is a generic representation of some lattice displacement around the defect. The exact nature of the lattice distortion need not be specified. The vertical axis represents the total energy around

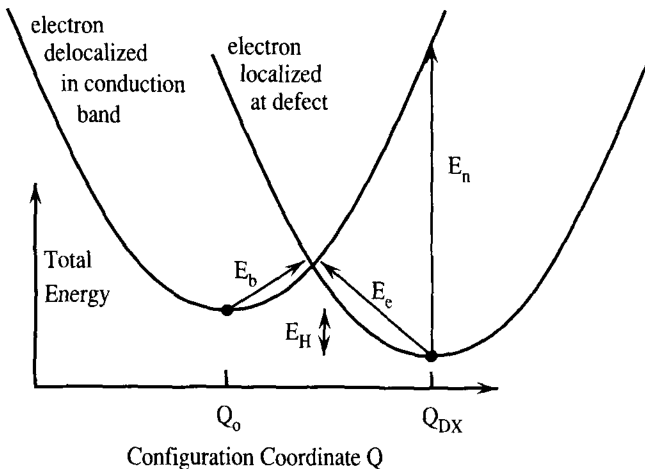

Fig. 3 — Configuration coordinate model for large lattice relaxation electron trapping at the *DX* center from Lang *et al.*[17] The vertical axis is the sum of the single electron energy plus the quadratic elastic deformation energy about the defect.

the defect, that is, the energy of the electronic state plus the lattice distortion energy resulting from the displacement. Q. The two parabolas represent two electronic states, a free electron in the lowest conduction band, and an electron bound to the *DX* center. The parabolic dependence of each results from a simple force constant representation of the lattice eneregy about an equilibrium point. The total energy difference between the two minima is the equilibrium binding energy E_H. The key feature of this model is that the equilibrium coordinates for the two states are significantly different, such that the curves cross at a point in between. If one assumes that the crossing point is the energy that must be achieved for thermally induced emission and capture, then E_e and E_b may be derived simply from the height of the crossing point, as shown in Fig. 3. The large optical ionization energy E_n comes naturally in this picture from the fact that optical transitions must be vertical, that is, for a fixed lattice configuration. Most of this energy goes to support the large lattice distortion at position Q_{DX}, and is subsequently released during relaxation to the equilibrium coordinate for the ionized state, Q_0. This relaxation energy is just the Frank-Condon energy. Quantitative values for E_n have been obtained from fits to $\sigma_n^o(h\nu)$, treating E_n and the local vibrational mode energy (in Q) as adjustable parameters. This simple model explained all of the relevant experimental features of the *DX* center, and has received wide acceptance.

PHOTOLUMINESCENCE, σ_n^o, AND A PROPOSED SMALL LATTICE RELAXATION MODEL

Recent renewed interest in the degree of lattice relaxation exhibited by the *DX* center was brought about by a two optical experiments on Si-doped $Al_xGa_{1-x}As$. The first was the observation of Henning *et al.*[21,22] of donor-to-acceptor transitions in low temperature photoluminescence, the deepest of which was interpreted as involving the *DX* center.[21,22] Figure 4 is a reproduction of one such spectrum from this work, showing the strong D^{Γ}-to-acceptor recombination along with a much weaker D^L-to-acceptor line referred to as D_4. A series of such measurements indicated that this donor (D_4) was approximately 200 meV below the conduction band edge, and was observed to approximately follow the L minimum for alloy compositions $0.25 < x < 0.60$, hence the D^L-to-acceptor designation. The D_4 line also exhibited local mode vibronic replicas parameterized by an energy of 48 meV and a Huang-Rhys parameter $S = 0.5$. The Huang-Rhys parameter is a measure of the number of "average" phonons emitted during capture or emission. For comparison, the LLR analysis based upon E_n ~1.0 eV yields a dominant phonon energy of ~9 meV and thus $S \sim 100$. The D_4 level is a donor, somewhat deeper than expected for an effective-mass-like impurity level, with only weak coupling to the lattice and a relatively high energy local vibrational mode en-

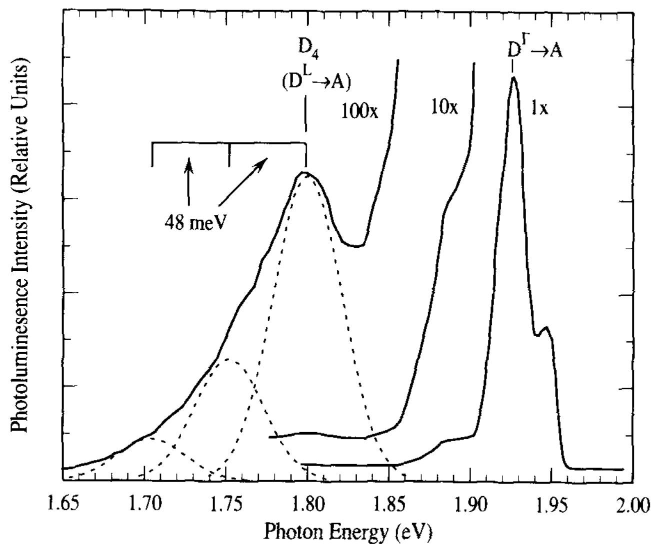

Fig. 4 — Low temperature photoluminesence spectrum of Si-doped, compensated $Al_{0.34}Ga_{0.66}As$ from Henning *et al.*[21] This optical emission is dominated by donor to acceptor transitions. Line D_4 follows the L-band edge with alloy composition variation, hence the D^L—A designation. The dashed Gaussians represent a deconvolution of D_4 into a no-phonon line and two replicas, at a 48 meV spacing.

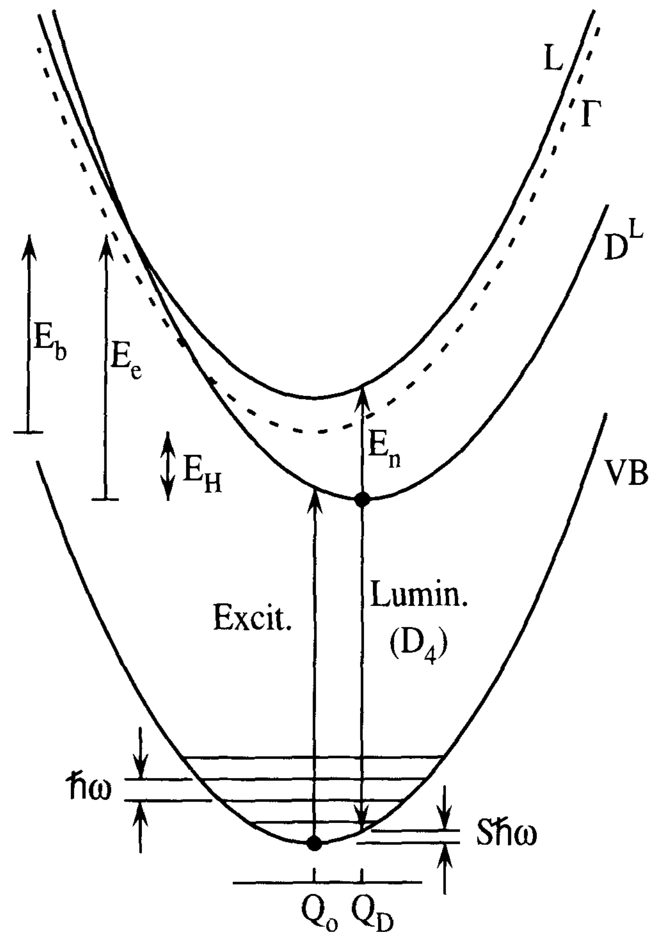

Fig. 5 — Configuration coordinate diagram for small lattice relaxation model proposed by Henning.[21] In the luminescence process, the initial hole state is really an acceptor level, which is at a fixed position above the valence band.

ergy. What was suggested, but not proved, was that the D_4 level was due to the same center as *DX*, if not the deep state, then perhaps a metastable shallower bound state of the same center.[22,24]

Based upon these photoluminescence data and existing data on thermal emission and capture, Henning *et al.*[21] proposed the small lattice relaxation model presented in Fig. 5. This configuration coordinate diagram shows the *L*-band free electron state (*L*) and the occupied donor state D^L as a function of a configuration coordinate Q. In contrast to the LLR model of Fig. 3, the lattice displacement $Q_D - Q_0$ is small, and the crossing of the occupied and free electron states occurs outside of, instead of between Q_D and Q_0. By suitable placement of the parabolas, the energies for thermal capture (E_b), thermal emission (E_e), and thermal equilibrium (E_H) can be made to fit the experimental data. Also shown is the free hole (VB) state, and the excitation process resulting in the D_4 luminescence line. The key difference between the predictions of this model and the LLR model is found in the optical ionization transition E_n, which should be ~0.2 eV, in contrast to greater than 1.0 eV for in the LLR model.

The above photoluminescence results clearly called for further exploration of the photo-ionization threshold for the *DX* center. If the occupied *DX* center underwent only small lattice relaxation upon ionization, then the lowest optical transition must be at a significantly lower energy than determined by Lang.[7] Henning *et al.*[23] carried out a photoionization experiment on Si-doped $Al_{0.33}Ga_{0.67}As$, utilizing the persistent change in conductivity, with a particular emphasis upon following the cross section to as small a value as possible. In their experiment, samples were cooled in the dark to 60 K and then exposed to an optical source consisting of a lamp followed by a series of filters that passed a narrow band at the desired energy. The rate of ionization was detected by the resulting rate of increase in the (persistent) conductivity of the sample. The energy dependence of the cross section measured in this manner is plotted in Fig. 6 as solid squares. The cross section varied by over five orders of magnitude from a maximum at 1.7 eV, and was claimed to be still detectable at photon energies as low as 0.25 eV. For comparison the continuous line is data from Lang *et al.*,[17] covering a much smaller dynamic range. Henning suggested that Lang's measurement, at least in the case of Si-doped $Al_xGa_{1-x}As$, was not of the threshold for ionization to the lowest conduction band edge, but rather to a higher band edge, and that the lowest energy photoionization process had a greatly reduced cross section and thus had not been detected by Lang. If this were the case, then the accepted picture of large lattice relaxation of the *DX* center would require significant reexamination.

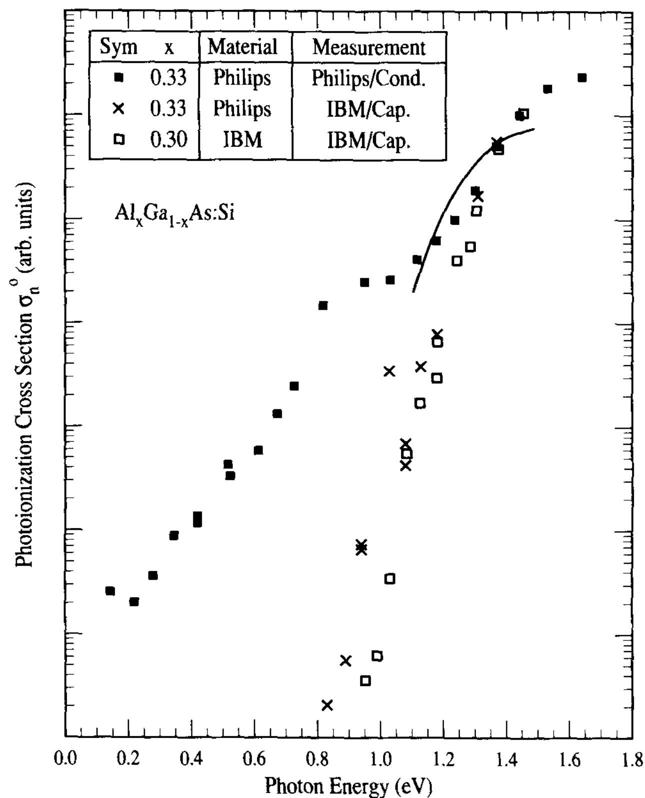

Fig. 6 — Comparison of photoionization cross sections from different publications. The solid squares are from reference,[23] and the open squares and x's from reference.[26] The solid squares and the x's were taken from different pieces of the same source material. The solid curve shows Lang's data[7,17] for comparison. The data are normalized at 1.4 eV.

LARGE DYNAMIC-RANGE MEASUREMENTS OF THE Si-*DX* CENTER

We have carried out extensive measurements of the *DX* center photoionization cross section σ_n^o,[26] using a photo-capacitance method similar to that used by Lang.[17] Three Si-doped (7×10^{16} cm^{-3}) 1.0 μm layers of Al mole fractions 0.30, 0.48, and 0.74 were grown by MBE, and Schottky diodes were formed in-situ by evaporation of 200Å semi-transparent Mo layers. A fourth sample ($x = 0.27$) was a modulation-doped FET with a 500Å $Al_xGa_{1-x}As$ layer Si-doped to 1×10^{18} cm^{-3}, also grown by MBE. These devices were cooled in the dark to 80 K while maintaining a 0.5 V forward bias, producing occupied *DX* centers throughout much of the active layer. The capacitance of the diodes (or of the gate of the FET) was detected by an a capacitance meter (PAR model 410), and during the transient measurements a feedback circuit was used to adjust the voltage to maintain a constant capacitance. This keeps the depletion depth within the diode constant, which is required to obtain exponential transients, since *DX* is the dominant trap in this material.[7,19] As optical ionization of *DX* centers proceeds within the space charge region of the diode, the feedback increases the voltage to compensate for the increased space charge density. The voltage is linear with the space charge density, and since the depletion width is kept constant, a fixed volume is sampled. However, with the *DX* centers initially fully occupied, as is the case when $x = 0.30$ and 0.48, the entire $Al_xGa_{1-x}As$ layer is depleted, resulting in a low value of C which is nearly independent of voltage. To obtain a larger capacitance which varies with the applied voltage, the diode was initialized by biasing at 0 V and exposure to light until an intermediate capacitance is reached, then the shutter closed and the feed-back activated to maintain that capacitance. The ionization rate was then detected as a voltage transient, with the degree of ionization being strictly proportional to the voltage change. This technique has the additional advantage that once exicted into the conduction band, the electrons are rapidly swept out of the space charge region, providing added assurance that they cannot be recaptured.

The optical portion of the experimental apparatus is outlined in Fig. 7. The sample was housed in a light-tight liquid-nitrogen-cooled cryostat with a single sapphire window covered by a manually operated shutter. The light source was either a tungsten lamp with narrow band filters, used at energies of 0.8 eV and above, or the tunable IR laser system indicated in Fig. 7 which provided a greater intensity in a much narrower bandwidth needed for the rapidly decreasing cross section below 1.2 eV. For most samples the lamp and filters were used only for energies greater than 1.2 eV. When using the laser system, the power was sampled at the time of the experiment by splitting part of the beam onto a Ge photodiode. The laser system is discussed in detail in the final section of this paper.

Full transients were recorded at a number of pho-

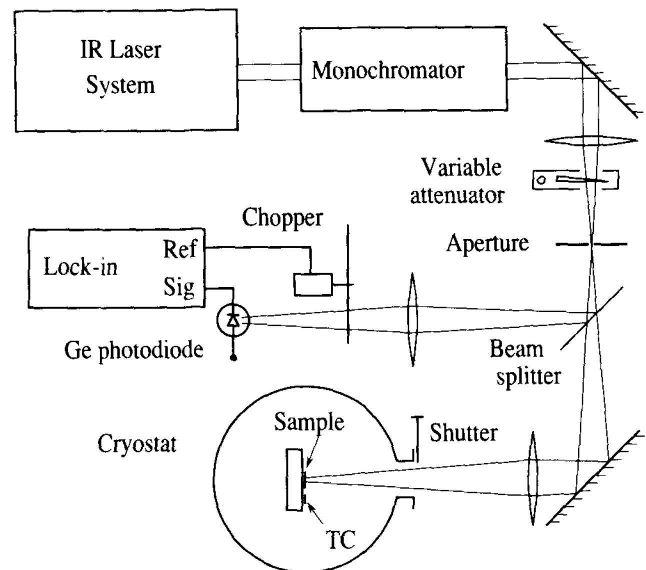

Fig. 7 — Block diagram of the optical portion of the photoionization measurement system. The OPO and monochrometer are the infra-red laser system described in the last section of this paper. The aperture, which was the same size as the samples, served to control the 1:1 transfer of the tightly focused laser beam onto the sample.

ton energies, and the amplitude was always the same, indicating that *DX* ionization is the dominant process at all energies. At an energy of 1.2 eV, a full transient required of order an hour to complete. Therefore, to obtain data at a reasonable rate, the initial slope of the transient ($\Delta V/\Delta t$) was normalized to the optical power density and taken as a relative measure of the *DX* center photoionization rate. In practice, each transient measured had a ΔV of around 0.3% of the voltage swing observed for a full transient after initialization, and no more than 10 such transients (3% cumulative) were recorded per cooling. After completion, the sample was raised to room temperature and then cooled again in the dark for the next series of measurements.

A summary of the data obtained for the four primary samples in this study is provided in Fig. 8. This includes data taken both with the lamp and with the IR laser system, plotted on a logarithmic scale, and normalized to the same value at 1.2 eV. A determination of the photon flux in the high energy range resulted in an estimated maximum of $\sigma_n^o = 1 \times 10^{-17}$ cm^{-2} at 1.9 eV. With all of the curves covering 7 to 8 orders of magnitude, the smallest detected cross section was of order 10^{-24} cm^{-2}. Although there is some variation in shape from sample to sample, no persistent ionization was detected at energies below 0.8 eV.

These results are in qualitative agreement with those of Lang, while they differ greatly with those of Henning, as may be seen in Fig. 6. This compares

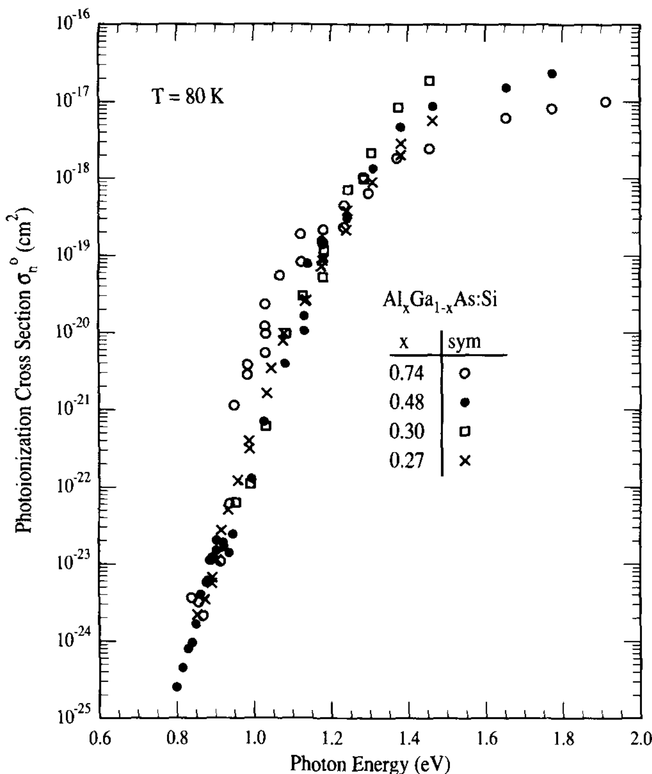

Fig. 8 — Composite plot of photoionization cross sections for samples with four different alloy compositions. The vertical axis is logarithmic, covering 9 orders of magnitude, and the curves are normalized at 1.3 eV.

our $x = 0.30$ sample with Henning's $x = 0.33$ sample, normalized at 1.4 eV. While the two results match well above 1.2 eV, the disagreement is severe below that. Our results show a single threshold, starting at ~0.9 eV. At this energy Henning shows a cross section 4 orders of magnitude higher, and at 0.2 eV his cross section is still above our detection limit. *Since we are secure in the fact that we are observing predominantly DX ionization above 1.0 eV, and see no ionization whatever below 0.8 eV, it is clear that Henning's result*[23] *is anomalous.* Potential causes of that anomalous result can be divided into 2 groups, problems associated with sample quality or electrical measurement technique, which will be discussed next, and problems associated with the optical source, discussion of which will be deferred to the next section.

In an attempt to determine whether the widely different results of Fig. 6 were due to sample differences, samples were exchanged between the Philips and IBM groups. Our applying the same methods described above to a piece of the $x = 0.33$ sample obtained from the Philips groups resulted in the x's in Fig. 6. In contrast to the data in Fig. 8, the spectrum for this sample appears not to be monotonically decreasing with energy. The suggestion of a shoulder at 1.0 eV may be connected a deep level that was observed in DLTS at 1.03 eV, at a density of 7.5×10^{-14} cm^{-3}. Although this curve is not identical to our original samples, there is a major discrepancy with respect to the photoconductivity results on the same material. We therefore reason that most of the difficulty with Henning's photoconductivity results lay in experimental procedure.

One possible source of these anomalous results could be a confusion of ionization of the *DX* state, which is a *persistent* effect, with small transients of a *nonpersistent* nature. Such transients were consistently observed in our three lower doped samples (7×10^{16} cm^{-3}) with an amplitude $\Delta V/V$ of order 10^{-3} to 10^{-4} of the *DX* transient. When the *DX* ionization rate was small and the photon flux was maximized this effect was quite significant. Figure 9 is an example of a transient that clearly shows both components. An initial fast transient occurring when the shutter is opened is followed by a slower and quite linear *DX* ionization process. The slope of this "slow" transient is denoted by the dashed line which represents the *DX* ionization rate. When the shutter is closed, there is a reversal of equal amplitude to the initial rise. Thus the fast transient is not persistent and does not arise from the deep *DX* state. Furthermore, this nonpersistent transient was seen in all three lower doped samples, but was not measurable in the MODFET, which was doped a factor of 15 higher. This indicates that the source of this signal does not scale with the doping (and hence the *DX* center) density.

In a later publication the Philips group did recognize these "fast" transients,[25] however, they did not address the question of whether they were a persistent effect or not. They did show that the "slow"

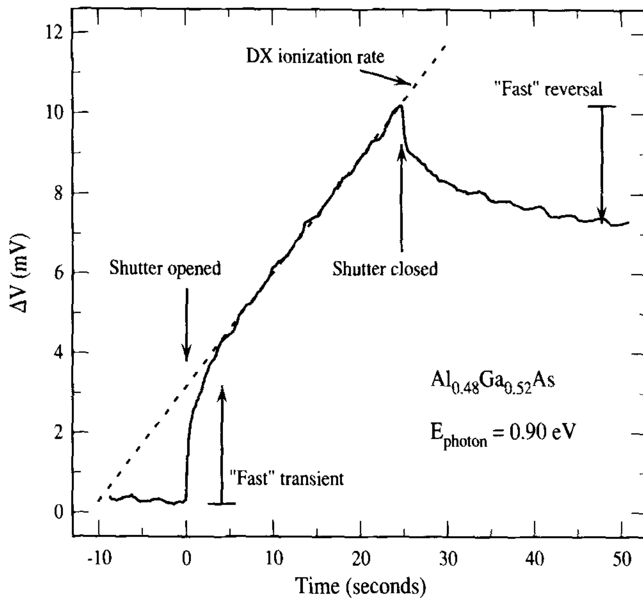

Fig. 9 — Optical ionization transient, showing both slow and fast components. The rise time of "fast" component is limited by the detection electronics.

ionization process had a threshold around 0.7 eV, while the "fast" process persisted at roughly a constant cross section down to around 0.3 eV. They suggested that if the *DX* center has a bi-stable ground (occupied) state then the slow transient could be ionization of the deep state and the fast one ionization of the shallow one. It is clear that both the D_4 photoluminescence and this nonpersistent photoionization represent real processes. However, it remains to be proven whether these optically shallow traps are a metastable configuration of the center responsible for *DX*, or are simply unrelated centers. In any case, it is clear that optical ionization from the deep *DX* state *requires* a large photon energy, *thus confirming unequivocally the large lattice relaxation model for this center.*

APPLICATION OF A TUNABLE INFRA-RED LASER SYSTEM TO PHOTOIONIZATION SPECTROSCOPY

Conventional (thermal) optical sources present two difficulties that can limit the dynamic range achieved in photo-ionization measurements. The first is the fundamentally limited brightness available in such sources makes the observed transient times very long as σ_n^o becomes vanishingly small near the threshold. A 3000 K black-body source filtered with 25% efficiency to a 10 meV bandwidth at 800 meV, with $f/2$ transfer optics, will result in a photon flux of $\sim 10^{17}$ photons-cm^{-2}-sec^{-1}. Estimates put the peak value of σ_n^o for the *DX* center at 10^{-17} cm^{-2}, which requires the detection of a cross section of 10^{-21} cm^{-2} to achieve a dynamic range of 10^4. For the above photon flux, this would require three hours to observe a full transient. The second problem encountered with a thermal source is the difficulty of adequately blocking the light at higher energies where σ_n^o is large. Better than 10^6/unit-bandpass rejection of light throughout the 1.0 to 1.5 eV range would be required to avoid inadvertent ionization by these photon energies. This is beyond the capabilities of conventional interference filters and single pass monochrometers, and could only be achieved by the careful application of multiple filters or multi-pass monochrometers. Even if the latter solutions provide the desired rejection, they will also further reduce the total optical throughput. Clearly the only reliable way to extend measurements of σ_n^o below the 10^{-21} level is to use a non-thermal, tunable source of infra-red radiation, *i.e.* a tunable IR laser.

While tunable dye lasers are widely available and highly practical in the visible and very near IR spectral ranges, their range hasn't been extended to wavelengths beyond 1.0 μm (<1.2 eV). At energies lower than this, the production of narrow-band tunable IR becomes much more difficult. There are two classes of laser system that will fit these requirements: 1) tunable solid state lasers (color center lasers), and 2) various nonlinear optical mixing techniques. At first glance, color center lasers may seem an ideal solution.[29] They are solid state analogs of dye lasers, utilizing lasing of the broadened defect luminescence bands found in many radiation damaged insulating crystals. They operate at wavelengths from around 1.0 μm to as long as 3.3 μm, exhibit very narrow bandwidth (10^{-5} eV), good output power (10 mW to 1 W), and are continuously tunable. Their principal disadvantage is that the tuning range for each crystal is only ~10% of the energy, and stable and reliable crystals do not exist for all spectral ranges. More specifically, there are no good crystals in the 1.1 μm to 1.4 μm range, which covers the threshold for photo-ionization of the Si related *DX* center in $Al_xGa_{1-x}As$. Furthermore, the wide spectral range (1.0 μm to 1.5 μm) covered in this work would require at least 3 crystal changes, which would make the measurements much more difficult. Color center lasers are more appropriate for spectroscopy of systems in more limited spectral ranges, and where their very narrow linewidth is required.

The second class of sources of IR, nonlinear mixing of shorter wavelength lasers, is more appropriate to semiconductor defect studies precisely because these techniques generally trade larger linewidth or lower power for increased flexibility and spectral coverage. In its most generic form, two laser beams are passed through a transparent crystal, and interact through the nonlinear susceptibility χ^2_{ijk} to produce some photons at the sum and/or difference energy of the two input beams. All that is required is that the instantaneous power density of the input beams is sufficiently high, that the beams overlap spatially, and that energy and wave-vector amongst the three waves are conserved. Generally, pulsed lasers are required to achieve a significant degree of conversion. One form of this is frequency summing, which is commonly used to double the energy of infrared lasers into the visible. Conversely, infrared may be generated at the difference energy of

two visible or near-IR beams. If one of the input beams is tunable, *i.e.* a dye laser, then the generated IR beam will likewise be tuned across an equal energy range. The simplest form this might take would be subtractive mixing of part of a fixed wavelength in the green (~500 nm) with a dye laser beam in the deep red (~730 nm). Although simple, this scheme is often limited in output power, not so much by the available peak pump powers, but by damage thresholds in the nonlinear crystals. Since the conversion efficiency is proportional to the power density of all three optical waves, it can be most readily improved by recirculation of the weakest of the three, without significantly increasing crystal damage. This is the basis for an optical parametric oscillator (OPO),[30] of which the system used in this work on the *DX* center is an example.

A block diagram for the OPO used in this study is shown in Fig. 10. The primary optical source is a copper vapor laser, which is a high repetition rate (5 kHz), pulse discharge laser with lines at 510 nm and 578 nm. The average power is 20 W, and the pulse duration is 30 ns. Both lines are used to pump a grating tuned flowing cell dye laser consisting of an oscillator followed by a single stage amplifier. Two dyes have been employed, R6g covering from 560 to 585 nm, and Kiton red covering the range 595 to 620 nm. This particular OPO scheme was developed by Wallace,[31] using a flash pumped dye laser. The only advantage of the system presented here is the much higher repetition rate and average power of the Cu vapor pumped system. The ~1 W output of the dye laser is used to coaxially pump the parametric oscillator through its dichroic back reflector, which is transmissive in the red, but a high reflector beyond 800 nm. This reflector, along with another IR reflector labeled output coupler in Fig. 10,

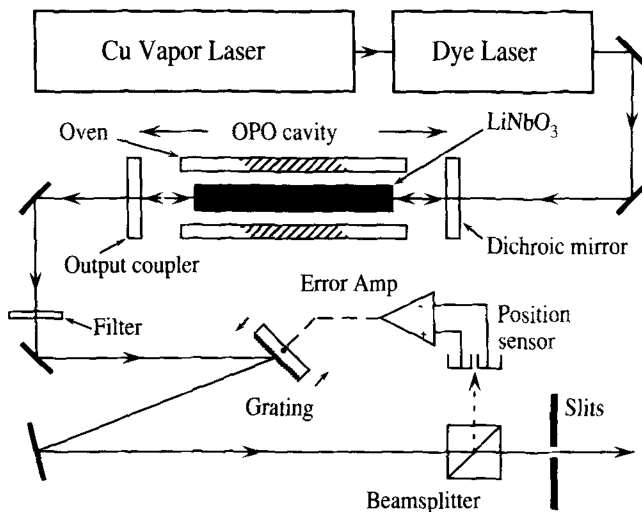

Fig. 10 — Tunable infra-red laser system used in this work. One of the two infrared beams (signal or idler) is selected and tracked by the grating, using position sensing and active feedback. Tuning is achieved by tuning the dye laser and determining the exact IR wavelength from the grating position.

form the cavity of the OPO. The conversion takes place in a 5 cm long *a*-axis $LiNbO_3$ crystal. The ends of this crystal are polished perpendicular to the optic axis, and it is heated in a temperature controlled oven into the range 200 to 350° C. The elevated temperature is required to avoid permanent damage to the $LiNbO_3$, and as will be shown below, is optimal for proper phase matching in the available dye wavelength ranges.

The basic nonlinear process in the $LiNbO_3$ is the conversion of one incident dye laser (pump) photon into two IR photons of equal total energy, referred to for historical reasons as the signal and idler. Conservation of energy for this process may be expressed as

$$\omega_p = \omega_s + \omega_i, \tag{1}$$

where ω is the frequency of each optical wave. In addition to the conservation of energy, a form of conservation of wave-vector is required for this parametric conversion process to occur. This can be written as:

$$\vec{k}_p = \vec{k}_s + \vec{k}_i, \tag{2}$$

where $\vec{k}$ is the wave-vector with magnitude $\omega n/c$. The index of refraction (n) relates the frequency to the wave-vector. In general, the index of refraction depends weakly on the frequency (ω) and the polarization (j). Thus, for colinear propagation of all three waves, wave-vector conservation may be rewritten as

$$\omega_p n_j(\omega_p) = \omega_s n_j(\omega_s) + \omega_i n_j(\omega_i). \tag{3}$$

Since the index of refraction is generally a monotonic function of ω over a typical range of interest, it becomes clear that colinear phase matching cannot take place for an isotropic crystal. However, this spectral dispersion can be compensated for in birefringent materials by appropriate selection of polarizations. The material used in this case, $LiNbO_3$, is negative uniaxial, which for propagation along the *a*-axis means the ordinary polarization (along the *c*-axis) has a larger index than the extraordinary polarization (along the second *a*-axis). If the pump beam polarization is ordinary and the signal and idler are both extraordinary, then phase matching can be achieved, and is given by

$$\omega_p n_o(\omega_p) = \omega_s n_e(\omega_s) + \omega_i n_e(\omega_i). \tag{4}$$

This equation and Eq. (1) together uniquely determine the signal and idler frequencies for a given pump frequency. Phase matching curves have been calculated from Sellmeier equations for $n_o(\omega,T)$ and $n_e(\omega,T)$ which have been fit to index of refraction data for $LiNbO_3$.[32] The results are plotted in Fig. 11 as signal and idler wavelength vs pump wavelength for a series of crystal temperatures. Rapid and continuous tuning of the OPO is achieved by tuning

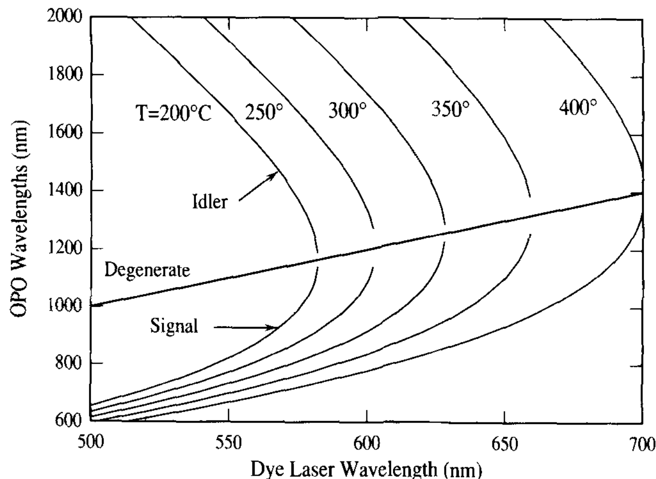

Fig. 11 — Tuning curves for the $LiNbO_3$ OPO. Operation is generally stable to within 5% of the degeneracy point. The resulting inaccessible region could then be reached by switching both dye and crystal temperature.

the dye laser, while different portions of the infrared may be reached for a given dye by changing the crystal temperature.

The idler is recirculated in the OPO cavity, achieving sufficient strength in all three fields for the gain to exceed the cavity loss for the idler, thus resulting in oscillation. This is known as a singly resonant oscillator (SRO). Doubly resonant oscillators (DRO's), which oscillate both the signal and the idler, have significantly lower pump thresholds, but also have greater problems with stability and continuous tunability. It is important that the OPO cavity be as short as possible, since oscillation needs to build up from the spontaneous parametric conversion limit within the 25 ns envelope of the dye laser pulse. In this case the cavity was 12.5 cm in length (optical length 18 cm), which provides about 20 forward gain passes through the $LiNbO_3$. The output coupler transmits most of the signal and enough of the idler for both to be available for experiments. This also means that for some experiments selection of one energy with high rejection of the other is important. This is the case for photoionization of the *DX* center when using the full intensity of the idler near the σ_n^o threshold. The grating filter shown in Fig. 10 performs this function, yielding a rejection of 5 to 6 orders of magnitude in the unwanted beam. Part of the output from the grating is split off and directed onto a position sensing Ge split-cell photodiode placed at a distance equivalent the exit slits. The signal from this sensor is proportional to the transverse position of the beam. The grating is mounted on a scanning galvanometer, and the signal from the position sensor is used, through a error-correction feedback circuit, to determine the grating position. In this way the grating filter can track the desired output beam continuously as the wavelength is varied, always keeping the beam centered on the position sensor and the output slits.

The application of the OPO system in measurements of σ_n^o for the *DX* center is diagrammed in Fig. 7. After exiting the tracking monochrometer, the beam is focused onto a 600 μm aperture, which is then focused 1:1 both onto the sample and onto a Ge photodiode via a beam splitter. This reference beam is chopped and measured by a lock-in amplifier, and calibrated by a themopile placed in the sample position. A variable attenuator placed before the beam splitter allowed control of the power from a few mW down to below 1 μW. Once measurement of a sample began, the projection of the aperture onto the sample was held fixed. Any drift in the position of the laser focus was corrected by translating the beam at the aperture to maximize throughput. This ensured a fixed coupling efficiency to the sample throughout a series of measurements.

CONCLUSIONS

We have reviewed the understanding of optical properties of the *DX* center in $Al_xGa_{1-x}As$, with a particular emphasis on the role that optical transitions play in elucidating the role of lattice relaxation at the defect. Data from our extended dynamic range photoionization cross section measurements are compared to results from two previous studies. We conclude that the photoionization process of the Si *DX* state requires an optical energy of at least 800 meV, and that there is no detectable ionization cross section at photon energies below 800 meV. Data from reference[23] does show a finite photoionization rate at energies as low as 200 meV, however, after an exchange of samples these results could not be reproduced. The conclusion is that the low energy photoionization process reported in reference[23] is attributable to some combination of two effects: 1) The optical source was not sufficiently intense and spectrally pure, thus the ionization observed was actually due to residual photons of energy greater than ~800 meV, and 2) The process observed at low energies was not ionization of the *DX* state. The latter possibility is enhanced by the use of photoconductivity to detect the ionization instead of photocapacitance. Therefore *all evidence points to an optical ionization energy for the deep DX state which is much larger than the thermal binding or emission energies.* This large Frank-Condon shift provides a point of distinction between large and small lattice relaxation models of the capture and emission process. The only model for capture and emission from the *DX* state which adequately explains both the thermal and the optical data involves large lattice relaxation around the defect in the process.

ACKNOWLEDGMENTS

We gratefully acknowledge the contributions of our collaborators on this work, T. N. Morgan and H. G. Grimmeiss. We also thank J. C. M. Henning for providing one of his samples. One of us (GAN) received support in part by the U.S. Office of Naval

Research under contracts N00014-85-C-0868 and N00014-90-C-0077.

REFERENCES

1. A. J. Springthorpe, F. D. King and A. Becke, J. Electron. Mater. *4,* 101 (1975).
2. P. K. Battacharya, U. Das and M. J. Ludowise, Phys. Rev. *B29,* 6623 (1984).
3. N. Chand, T. Henderson, J. Klem, T. Masselink, R. Fisher, Y. C. Chang and H. Morkoc, Phys. Rev. *B30,* 4481 (1984).
4. T. Ishikawa, K. Kondo, S. Hiyamizu and A. Shibatomi, Jpn. J. Appl. Phys. *24,* L408 (1985).
5. M. O. Watanabe, K. Morizuka, MN. Mashita, Y. Askizawa and Y. Zota, Jpn. J. Appl. Phys. *23,* L103 (1984).
6. H. Künzel, K. Ploog, K. Wünstel and B. L. Zhou, J. Electron. Mater. *13,* 281 (1984).
7. D. V. Lang, R. A. Logan and M. Jaros, Phys. Rev. *B19,* 1015 (1979).
8. R. J. Nelson, Appl. Phys. Lett. *31,* 351 (1977).
9. T. N. Theis, P. M. Mooney and S. Wright, Phys. Rev. Lett. *60,* 361 (1988).
10. M. Mizuta, M. Tachikawa, H. Kukimoto and S. Minomura, Jpn. J. Appl. Phys. *24,* L143 (1985).
11. M. Tachikawa, T. Fujisawa, H. Kukimoto, A. Shibata, G. Oomi and S. Minomura, Jpn. J. Appl. Phys. *24,* L893 (1985).
12. E. R. Li, E. R. Yu, E. R. Weber and W. Hansen, Phys. Rev. *B36,* 4531 (1987).
13. D. J. Chadi and K. J. Chang, Phys. Rev. *B39,* 10063 (1989).
14. K. Khachaturyan, E. R. Weber, and M. Kaminska, Mater. Sci. Forum (Switzerland) *38–41,* 1067 (1989).
15. K. Khachaturyan, D. D. Awschlom, J. R. Rozen and E. R. Weber, Phys. Rev. Lett. *63,* 1311 (1989).
16. M. G. Craford, G. E. Stillman, J. A. Rossi and N. Holonyak, Phys. Rev. *168,* 867 (1968).
17. D. V. Lang and R. A. Logan, Inst. Phys. Conf. Ser. *43,* 433 (1979).
18. D. V. Lang and R. A. Logan, Phys. Rev. Lett. *39,* 635 (1977).
19. D. V. Lang, Deep Centers in Semiconductors (Gordon and Breach Science Publishers, New York, 1986), pp. 489–539.
20. D. V. Lang, J. Phys. Soc. Japan *49 Suppl. A,* 215 (1980).
21. J. C. Henning and J. P. Ansems, Semicond. Sci. Technol. *2,* 1 (1987).
22. J. C. Henning, J. P. Ansems, and P. J. Roksnoer, Semicond. Sci. Technol. *3,* 361 (1987).
23. J. C. Henning and J. P. Ansems, Appl. Phys. A. *44,* 245 (1987).
24. J. C. Henning, E. A. Montie and J. P. Ansems, Mater. Sci. Forum (Switzerland) *38–41,* 1085 (1989).
25. J. C. Henning and J. P. Ansems, Phys. Rev. *B38,* 5772 (1988).
26. P. M. Mooney, G. A. Northrop, T. N. Morgan and H. G. Grimmeiss, Phys. Rev. *B37,* 8298 (1988).
27. P. M. Mooney, N. S. Caswell and S. L. Wright, J. Appl. Phys. *62,* 4786 (1987).
28. M. Jaros, Phys. Rev. *B16,* 3694 (1978).
29. L. Mollenauer, Tunable Lasers (Springer-Verlag, 1987).
30. R. G. Smith, Lasers: A Series of Advances (Marcel Dekker, New York, 1976), pp. 189–307.
31. R. W. Wallace, IEEE J. Quant. Elect. *QE-8,* 819 (1972).
32. M. V. Hobden and J. Warner, Physics Lett. *22,* 243 (1966).